

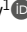


ARTICLE

# Engineered high-affinity zinc binding site reveals gating configurations of a human proton channel

Vladimir V. Cherny<sup>1</sup>, Boris Musset<sup>2</sup> , Deri Morgan<sup>1</sup> , Sarah Thomas<sup>3</sup>, Susan M.E. Smith<sup>3</sup>, and Thomas E. DeCoursey<sup>1</sup> 

The voltage-gated proton channel (H<sub>v</sub>1) is a voltage sensor that also conducts protons. The singular ability of protons to penetrate proteins complicates distinguishing closed and open channels. When we replaced valine with histidine at position 116 in the external vestibule of hH<sub>v</sub>1, current was potently inhibited by externally applied Zn<sup>2+</sup> in a construct lacking the two His that bind Zn<sup>2+</sup> in WT channels. High-affinity binding with profound effects at 10 nM Zn<sup>2+</sup> at pH<sub>o</sub> 7 suggests additional groups contribute. We hypothesized that Asp<sup>185</sup>, which faces position 116 in our closed-state model, contributes to Zn<sup>2+</sup> chelation. Confirming this prediction, V116H/D185N abolished Zn<sup>2+</sup> binding. Studied in a C-terminal truncated monomeric construct, V116H channels activated rapidly. Anomalous, Zn<sup>2+</sup> slowed activation, producing a time constant independent of both voltage and Zn<sup>2+</sup> concentration. We hypothesized that slow turn-on of H<sup>+</sup> current in the presence of Zn<sup>2+</sup> reflects the rate of Zn<sup>2+</sup> unbinding from the channel, analogous to drug-receptor dissociation reactions. This behavior in turn suggests that the affinity for Zn<sup>2+</sup> is greater in the closed state of hH<sub>v</sub>1. Supporting this hypothesis, pulse pairs revealed a rapid component of activation whose amplitude decreased after longer intervals at negative voltages as closed channels bound Zn<sup>2+</sup>. The lower affinity of Zn<sup>2+</sup> in open channels is consistent with the idea that structural rearrangements within the transmembrane region bring Arg<sup>205</sup> near position 116, electrostatically expelling Zn<sup>2+</sup>. This phenomenon provides direct evidence that Asp<sup>185</sup> opposes position 116 in closed channels and that Arg<sup>205</sup> moves between them when the channel opens.

## Introduction

Voltage-gated proton channels (H<sub>v</sub>1s) are widely distributed both phylogenetically and among different human cells (DeCoursey, 2013). An overview of the human H<sub>v</sub>1 (hH<sub>v</sub>1) dimer is shown in Fig. 1. The gating of H<sub>v</sub>1 remains a highly controversial and mysterious process. Largely by analogy with the voltage-sensing domain (VSD) of other voltage-gated ion channels, the S4 helix in H<sub>v</sub>1 has been presumed to move outward during channel opening. This historical bias persists, despite the fact that in contrast with other channels in which VSD movement must pull open a physically distant pore formed by the S5-S6 helices, in H<sub>v</sub>1 the conduction pathway resides within the VSD, thereby obviating any a priori need for a large conformational change (DeCoursey, 2015b). The extent of S4 movement in H<sub>v</sub>1 has been modeled as one (Kulleperuma et al., 2013; Li et al., 2015; van Keulen et al., 2017) to three “clicks” or helical turns (Ramsey et al., 2010; Randolph et al., 2016), as well as intermediate values (Wood et al., 2012; Chamberlin et al., 2015; Gianti et al., 2016). The strongest type of evidence that S4 actually moves comes from differences in accessibility of specific sites in closed and open channels. Studies introducing Cys into S4 and

probing with MTS reagents (Gonzalez et al., 2010) or introducing His into S4 and probing with Zn<sup>2+</sup> (Kulleperuma et al., 2013; Morgan et al., 2013) appear to indicate that S4 moves outward at least one click. This class of evidence has been questioned because of the different side-chain volumes occupied by introduced amino acids (Kariev and Green, 2018). In addition, mutations neutralizing charged residues in S4 appear to alter gating movements (Gonzalez et al., 2013). Given these considerations, it would be useful to evaluate gating using probes directed toward other less mobile parts of the channel molecule. We were especially interested in identifying positions at which an engineered metal-binding site was differentially accessible to metals in closed and open channels. The approach of introducing metal-binding sites to assess state-dependent binding has been used successfully in other voltage-gated ion channels (Webster et al., 2004; Lee and MacKinnon, 2019). In this effort, we discovered a location where introduction of a single His produced extraordinary sensitivity of the channel to Zn<sup>2+</sup>.

Externally applied Zn<sup>2+</sup> inhibits WT proton currents potently (Thomas and Meech, 1982; Mahaut-Smith, 1989b; Eder et al.,

<sup>1</sup>Department of Physiology & Biophysics, Rush University, Chicago IL; <sup>2</sup>Institut für Physiologie und Pathophysiologie, Paracelsus Medizinische Privatuniversität, Nürnberg, Germany; <sup>3</sup>Department of Molecular and Cellular Biology, Kennesaw State University, Kennesaw, GA.

Correspondence to Thomas E. DeCoursey: [tdcour@rush.edu](mailto:tdcour@rush.edu); D. Morgan's present address is University of Kansas Medical Center, Kansas City, MO.

© 2020 Cherny et al. This article is distributed under the terms of an Attribution-Noncommercial-Share Alike-No Mirror Sites license for the first six months after the publication date (see <http://www.rupress.org/terms/>). After six months it is available under a Creative Commons License (Attribution-Noncommercial-Share Alike 4.0 International license, as described at <https://creativecommons.org/licenses/by-nc-sa/4.0/>).

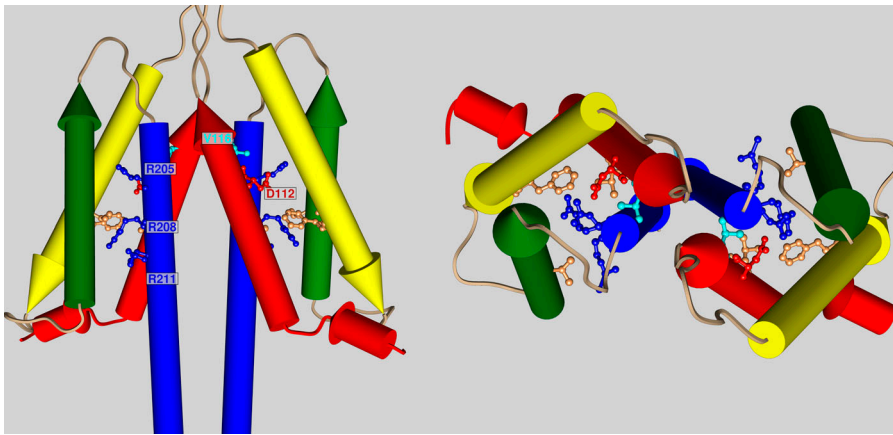


**Figure 1. Location of key amino acids in an hHv1 dimer model.** Homology model of the closed hHv1 dimer (Li et al., 2015) is shown in side view (left) and top view (right), where top corresponds to the extracytoplasmic side. Transmembrane helices are shown as pipes; connecting loops are shown as ribbons. The S1, S2, S3, and S4 helices are indicated in red, yellow, green, and blue, respectively. The hydrophobic gasket residues V109 (on S1), F150 (on S2), and V177 and V178 (on S3) are indicated in brown ball-and-sticks. Note that for clarity the side view is truncated above the strongest coiled-coil interaction of the C termini of the protomers.

1995; DeCoursey, 2003), with pronounced effects in mammalian cells at external pH,  $\text{pH}_o$  7 occurring at 1  $\mu\text{M}$  or higher (Schrenzel et al., 1996; Cherny and DeCoursey, 1999; Lishko et al., 2010). In addition to decreasing the maximum proton conductance ( $g_H$ ), divalent metal cations prominently shift the  $g_H$ -V relationship of native proton currents positively and slow activation (Barish and Baud, 1984; Byerly et al., 1984; Cherny and DeCoursey, 1999; Chaves et al., 2020). Both of these effects are strongly inhibited at low  $\text{pH}_o$ , and quantitative modeling of the competition between  $\text{Zn}^{2+}$  and  $\text{H}^+$  suggested that each  $\text{Zn}^{2+}$  ion binds to a site composed of at least two titratable groups with  $\text{pK}_a$  6.5–7.0, most likely His ( $\text{pK}_a$  is the pH at which half the groups are protonated; Cherny and DeCoursey, 1999). This prediction was confirmed when the *HVCN1* gene was identified and found to contain two externally accessible His (His<sup>140</sup> and His<sup>193</sup>); most of the inhibition of  $\text{H}_v1$  by  $\text{Zn}^{2+}$  is eliminated by mutating two  $\text{Zn}^{2+}$ -binding His in the H140A/H193A double mutant (Ramsey et al., 2006). The crystal structure of the mouse proton channel, mHv1, contained a  $\text{Zn}^{2+}$  atom near His<sup>136</sup> (His<sup>140</sup> in hHv1) and was consistent with its interaction also with His<sup>189</sup> (His<sup>193</sup> in hHv1), which was, however, disordered and not resolved (Takeshita et al., 2014).

Here, we show that the effects of  $\text{Zn}^{2+}$  on V116H mutants were strikingly different from those on WT channels. We introduced this mutation into a background (H140A/H193A) in which we replaced the two His that comprise the main binding site for  $\text{Zn}^{2+}$  in WT channels (Ramsey et al., 2006; Musset et al., 2010b; Takeshita et al., 2014). A single His introduced at position 116 in the outer vestibule bound  $\text{Zn}^{2+}$  with an affinity many orders of magnitude greater than His in bulk solution or than the background construct (H140A/H193A). The extremely high affinity suggests that other groups contribute to  $\text{Zn}^{2+}$  binding. We identify Asp<sup>185</sup> as providing an essential group.

The WT  $\text{H}_v1$  channel in humans and many other species exists as a dimer in the plasma membrane (Koch et al., 2008; Lee et al., 2008; Tombola et al., 2008), illustrated in Fig. 1. Several lines of evidence indicate that interactions between the two protomers in the dimer during channel opening produce cooperative gating (Gonzalez et al., 2010; Musset et al., 2010b; Tombola et al., 2010). In some studies, we also removed the C terminus (H140A/H193A/T222stop) to preclude the possibility of interactions between protomers during gating. Serendipitously,

because monomeric  $\text{H}_v1$  opens much faster than the WT dimeric form, introducing V116H into this background revealed two components of apparent activation. Analysis of the kinetics indicated that  $\text{Zn}^{2+}$  binds mainly to closed channels and is expelled from the channel when it opens. This behavior provides clues to the closed and open structures and constrains the opening mechanism of hHv1.

## Materials and methods

### Gene expression

Site-directed mutants were created using the Stratagene Quik-Change (Agilent) procedure according to the manufacturer's instructions. Transfection into HEK-293 cells was done as described (Kulleperuma et al., 2013). No other voltage- or time-dependent conductances were observed under the conditions of this study. The level of expression of the mutants studied here was sufficiently high that contamination by native  $\text{H}_v1$  was negligible.

### Electrophysiology

In most experiments, cells expressing GFP-tagged proton channels were identified using Nikon inverted microscopes with fluorescence capability. For constructs that lacked the GFP tag, GFP was cotransfected. Conventional patch-clamp techniques were used (Kulleperuma et al., 2013) at room temperature (20–26°C). Bath and pipette solutions contained 60–100 mM buffer, 1–2 mM  $\text{CaCl}_2$  or  $\text{MgCl}_2$  (intracellular solutions were  $\text{Ca}^{2+}$ -free), 1–2 mM EGTA, and TMAMeSO<sub>3</sub> to adjust the osmolality to ~300 mOsm, titrated with tetramethylammonium hydroxide (TMAOH). Buffers used were Homopipes at pH 5.0, Mes at pH 5.5–6.0, BisTris at pH 6.5, and PIPES at pH 7.0. Currents are shown without leak correction. To minimize changes in intracellular pH ( $\text{pH}_i$ ) due to large  $\text{H}^+$  fluxes, pulses for large depolarizations in pulse families were sometimes shortened.

We calculated free  $\text{Zn}^{2+}$  concentrations,  $[\text{Zn}^{2+}]$ , using WEB-MAXC STANDARD from the MaxChelator series (Bers, 2009). This venerable program is currently based in the University of California at Davis, Davis, CA. We appreciate the help of Donald M. Bers, Eleonora Grandi, Brittany C. Kolb, and Daniel Cotton in facilitating access. The program includes metal and proton binding to buffers as a function of temperature and ionic strength.

Proton current amplitude ( $I_H$ ) was usually determined by fitting the rising current with a single exponential and extrapolating to infinite time.  $g_H$  was calculated from  $I_H$ , and the reversal potential,  $V_{rev}$ , was measured in each solution:  $g_H = I_H / (V - V_{rev})$ .  $V_{rev}$  was determined by two methods, depending on the relative positions of  $V_{rev}$  and the threshold voltage for activation of the  $g_H$ ,  $V_{threshold}$ . For constructs in which  $V_{threshold}$  was positive to  $V_{rev}$ , the latter was determined by examining tail currents. Because hHv1 currents were the only time-dependent conductance present,  $V_{rev}$  was established by the amplitude and direction of current decay during deactivation. By using this procedure, a time-independent leak or other extraneous conductances do not affect  $V_{rev}$ . Tail currents were not observed in nontransfected cells. For mutants in which  $V_{threshold}$  was negative to  $V_{rev}$ , it was possible to observe directly the reversal of currents activated during pulse families.

## Results

### Part I: Experiments on dimeric channels

#### V116H mutant is potentially inhibited by $Zn^{2+}$

To observe in isolation the effects of  $Zn^{2+}$  binding to a His introduced at position 116 (V116H), we first eliminated the two His that bind  $Zn^{2+}$  in WT hHv1 (Ramsey et al., 2006). Fig. 2 A shows that this  $Zn^{2+}$ -insensitive construct (H140A/H193A) is only weakly inhibited by 100  $\mu M$   $Zn^{2+}$ , with more significant inhibition at 1 mM. Consequently, the effects of  $Zn^{2+}$  described below at lower concentrations are due almost entirely to the presence of His at position 116. The kinetics of activation is not noticeably affected by removal of these two His (Fig. 3). The most obvious effects of  $Zn^{2+}$  on the  $Zn^{2+}$ -insensitive background construct are decreased current amplitude and a positively shifted  $g_H$ -V relationship, with little change in kinetics. In this  $Zn^{2+}$ -insensitive background, introducing a single His at position 116 in the outer vestibule (V116H) increased the  $Zn^{2+}$  affinity drastically. Fig. 2 B shows that 10 nM  $Zn^{2+}$  profoundly inhibited  $H^+$  currents at pH<sub>o</sub> 7. The current amplitude was reduced, activation kinetics was slowed, and the  $g_H$ -V relationship was shifted positively, with larger effects on all three parameters at 100 nM  $Zn^{2+}$ . Qualitatively, these effects recapitulate the manifestations of  $Zn^{2+}$  inhibition of Hv1 in most mammalian cells (Cherny and DeCoursey, 1999), although the reduction of current amplitude appeared much more prominent than is observed in WT Hv1 channels. The affinity of this engineered  $Zn^{2+}$  binding site was so high that simply adding EGTA to nominally  $Zn^{2+}$ -free solutions relieved inhibition by unknown contaminants, presumably polyvalent metal cations. High-affinity  $Zn^{2+}$  binding sites exist in NMDA receptors, where a similar problem of heavy metal contamination of standard solutions was encountered (Paoletti et al., 1997). To establish a defined low concentration of free  $Zn^{2+}$ ,  $[Zn^{2+}]$ , the solutions in Fig. 2 B were buffered with ADA (*N*-(2-Acetamido)iminodiacetic acid, *N*-(carbamoylmethyl)iminodiacetic acid), with  $[Zn^{2+}]$  calculated using WEBMAXC STANDARD from the MaxChelator series (Materials and methods).

Fig. 4 illustrates that the single added His in V116H increased  $Zn^{2+}$  sensitivity, assessed by the reduction of current at +60 mV,

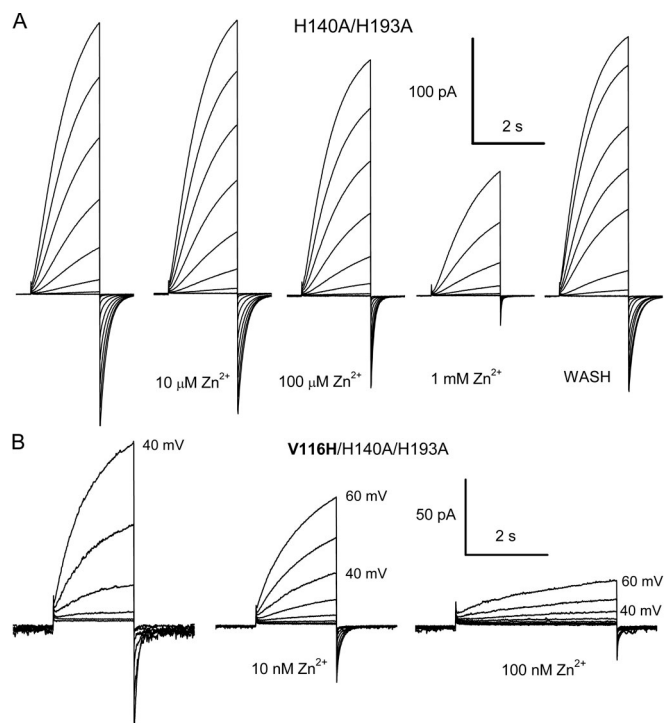


**Figure 2.  $Zn^{2+}$  binds very weakly to hHv1 with His<sup>140</sup> and His<sup>193</sup> removed, but with extraordinarily high affinity when His is introduced at position 116 (V116H).** (A) The H140A/H193A background for dimer studies lacks the two His critical for  $Zn^{2+}$  binding and is insensitive to  $Zn^{2+}$  up to 100  $\mu M$ . Families of currents in 10-mV increments up to +40 mV are shown for the indicated concentrations of  $Zn^{2+}$ , all at pH<sub>o</sub> 7, pH<sub>i</sub> 6.5. (B) Extreme  $Zn^{2+}$  sensitivity of V116H mutant in the H140A/H193A background. Families of currents at pH<sub>o</sub> 7, pH<sub>i</sub> 7 showing that 10 nM  $Zn^{2+}$  produces distinct inhibition. It is evident that in addition,  $\tau_{act}$  is slowed and the  $g_H$ -V relationship is shifted positively.

by 5–6 orders of magnitude compared with the background double His mutant H140A/H193A. In fact, V116H is >100-fold more sensitive to  $Zn^{2+}$  than is WT hHv1. To avoid the necessity of using buffered solutions for low  $Zn^{2+}$  concentrations, in many experiments we lowered the  $Zn^{2+}$  affinity by using pH<sub>o</sub> 6 solutions. The V116H mutant was distinctly less sensitive to  $Zn^{2+}$  at pH<sub>o</sub> 6 (Fig. 4, open symbols and dashed lines) than at pH<sub>o</sub> 7, as was WT hHv1. The inhibition of rat proton currents by  $Zn^{2+}$  was found previously to be extremely sensitive to pH<sub>o</sub>, with lower affinity at lower pH<sub>o</sub>, which was explained by  $Zn^{2+}$  competing with  $H^+$  for two or more titratable groups (Cherny and DeCoursey, 1999).

#### Location of Val<sup>116</sup> in closed and open hHv1: What helps V116H bind $Zn^{2+}$ ?

The affinity of  $Zn^{2+}$  for His in solution is rather weak,  $K_d$  at pH 7.4, 25°C, and 0.1 M ionic strength is 322  $\mu M$  (Krężel and Maret, 2016). The extraordinarily high affinity of  $Zn^{2+}$  for V116H strongly suggests that additional coordinating groups exist near this location and that steric factors are favorable. Examination of a closed state model of hHv1 (Li et al., 2015) reveals that Asp<sup>185</sup> is directly across the pore from position 116 (Fig. 5 A). To test whether Asp<sup>185</sup> indeed contributes to the coordination of  $Zn^{2+}$ ,



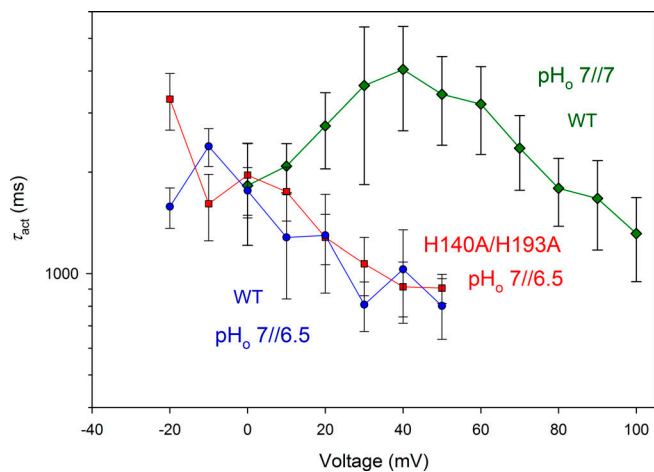


**Figure 3. The kinetics of activation is not changed in the  $\text{Zn}^{2+}$ -insensitive H140A/H193A mutant.** Turn-on of current was fitted with a single exponential. Direct comparison at  $\text{pH}_o$  7 and  $\text{pH}_i$  6.5 is shown, along with  $\text{pH}$  7/7 WT data (from Cherny et al., 2015) for reference. Mean  $\pm$  SEM is plotted for numbers of cells from negative to positive voltages: WT 5, 10, 12, 11, 11, 9, 10, and 3; and H140A/H193A 4, 6, 9, 9, 6, 6, and 4. Although the values at  $-20$  mV are just “significantly” different at  $P = 0.026$ , this is obviously a statistical aberration.

we replaced this Asp with Asn, which is similar in size but lacks a negative charge. The V116H/H140A/D185N/H193A mutant (D185N) generated robust currents (Fig. 6) that were only weakly sensitive to  $\text{Zn}^{2+}$  either at  $\text{pH}_o$  7 (Fig. 6, A–C) or at  $\text{pH}_o$  6 (Fig. 6, D–F).  $\text{Zn}^{2+}$  begins to inhibit proton currents in this construct only at  $100 \mu\text{M}$  at  $\text{pH}_o$  7 and at  $1 \text{ mM}$  at  $\text{pH}_o$  6 (Fig. 6 C and Fig. 4 F, respectively). The inhibition by  $\text{Zn}^{2+}$  is compared with WT and the  $\text{Zn}^{2+}$ -insensitive background construct (H140A/H193A) in Fig. 4. Combined with D185N, V116H may exhibit some anemic residual  $\text{Zn}^{2+}$  binding capability because it appears slightly more sensitive than the background construct. Nevertheless, it is evident that the potent  $\text{Zn}^{2+}$ -binding capability of His<sup>116</sup> strictly requires Asp<sup>185</sup> to facilitate coordination.

## Part II: Experiments on monomeric channels

The WT hHv1 channel exists as a dimer (Koch et al., 2008; Lee et al., 2008; Tombola et al., 2008), and interactions between the two protomers are thought to produce cooperative gating during channel opening (Gonzalez et al., 2010; Musset et al., 2010b; Tombola et al., 2010). To preclude complications resulting from inter-protomer interactions, we removed the C terminus as well as the two  $\text{Zn}^{2+}$ -binding His (H140A/H193A/T222stop) to produce mainly monomeric channels (Koch et al., 2008; Tombola et al., 2008; Musset et al., 2010b; Fujiwara et al., 2013). The  $\text{Zn}^{2+}$  sensitivity of this background construct (Fig. 7) was similar to that of the dimeric double mutant (H140A/H193A; Fig. 2 A); it was insensitive to  $10 \mu\text{M}$   $\text{Zn}^{2+}$ , with higher concentrations decreasing the current and shifting the  $g_{\text{H}}\text{-V}$  relationship positively, but with little effect on kinetics.

Next, we introduced His at position 116. Mammalian proton currents have notoriously slow opening kinetics, with activation time constants ( $\tau_{\text{act}}$ ) of 1–10 s at room temperature. Monomeric constructs have activation kinetics 3–17 times more rapid than

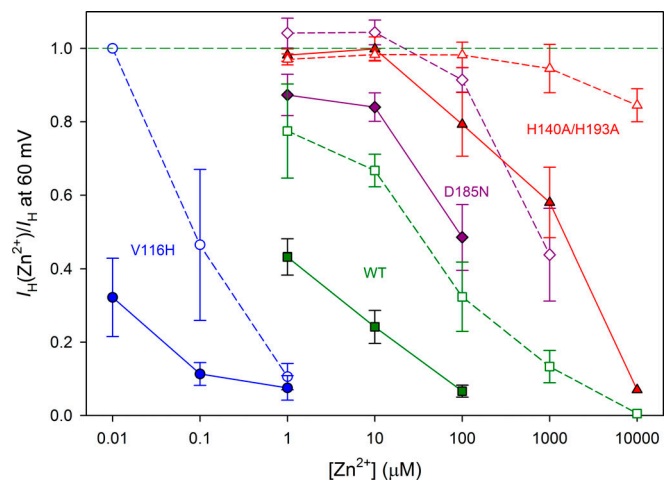


**Figure 4. Comparison of  $\text{Zn}^{2+}$  inhibition of proton current in V116H, D185N, and WT hHv1 and in the  $\text{Zn}^{2+}$ -insensitive H140A/H193A background.** Inhibition of  $\text{H}^+$  current by  $\text{Zn}^{2+}$  at  $+60$  mV in the V116H/H140A/H193A mutant (●), WT hHv1 (■), V116H/H140A/D185N/H193A (◆), and background construct H140A/H193A (▲). The mean  $\pm$  SEM ratio of test pulse current in the presence of  $\text{Zn}^{2+}$  to its absence is plotted. Solid symbols and lines show measurements at  $\text{pH}_o$  7, open symbols and dashed lines at  $\text{pH}_o$  6. For concentrations  $<1 \mu\text{M}$ ,  $\text{Zn}^{2+}$  was buffered with ADA. Numbers of cells, from low to high  $[\text{Zn}^{2+}]$ , for V116H are 6, 3, and 6 at  $\text{pH}_o$  7; 3, 3, and 8 at  $\text{pH}_o$  6; for WT 13, 10 and 7 at  $\text{pH}_o$  7; 4, 6, 5, 4, and 1 at  $\text{pH}_o$  6; for V116H/D185N 3, 4, and 4 at  $\text{pH}_o$  7; 4, 4, 4, and 3 at  $\text{pH}_o$  6; and for H140A/H193A 2, 5, 6, 4, and 1 at  $\text{pH}_o$  7; 3, 3, 3, 3, and 3 at  $\text{pH}_o$  6.

the WT dimer (Koch et al., 2008; Tombola et al., 2008; Musset et al., 2010b; Fujiwara et al., 2013). Accordingly, the monomeric construct activated rapidly (Fig. 8, red symbols), as is evident by inspection of Fig. 2 A and Fig. 7. The V116H mutation itself apparently accelerated channel opening in the dimeric construct (Fig. 8, blue symbols). Much of this speeding is due to the lower  $\text{pH}_i$  6 in these studies, however. The single mutant V116H in WT background (all His intact) at  $\text{pH}_o$  7,  $\text{pH}_i$  7 is only twice faster (Fig. 8, purple hexagons). Activation was not only rapid, but it also exhibited very little voltage dependence in the monomer. Kinetics was somewhat faster at  $\text{pH}_o$  7 than 6, consistent with typical WT hHv1 behavior.

Although the V116H mutation and monomerization of Hv1 both speed activation, it is unlikely that the V116H mutation itself produces monomerization. The dimer is stabilized by coiled-coil interactions at the C terminus (Koch et al., 2008; Lee et al., 2008; Tombola et al., 2008; Fujiwara et al., 2012, 2014), which remains intact. Position 116 faces the aqueous vestibule (Fig. 1 and Fig. 5) and is not well positioned to participate in any proposed dimer interface (Lee et al., 2008; Musset et al., 2010a, 2010b; Takeshita et al., 2014). Finally, Hv1 may differ from other voltage-gated ion channels by virtue of the observation that gating kinetics was altered by nearly all point mutations in which it was studied (DeCoursey et al., 2016).

## $\text{Zn}^{2+}$ has qualitatively different effects on the V116H monomer than on WT channels

Families of currents generated by the V116H monomer (V116H/H140A/H193A/T222stop) are shown in Fig. 9. Row A is at  $\text{pH}_o$  6,

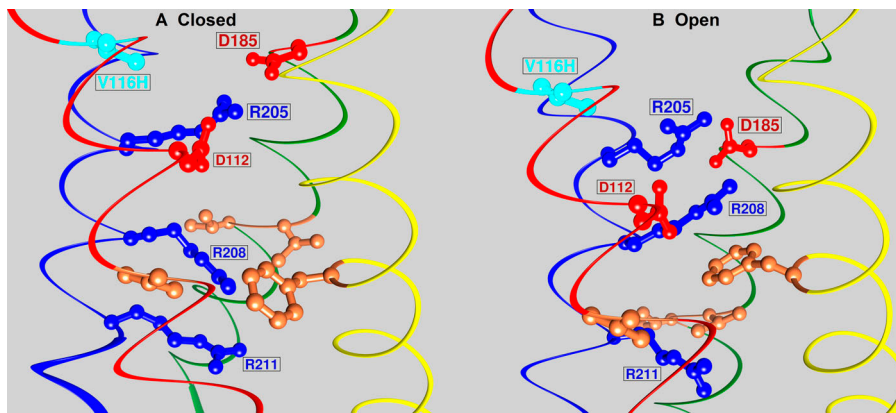


**Figure 5. Map of key amino acids in closed and open hHv1 models.** (A and B) Alpha carbons of S2 helices (yellow ribbon) of closed (A, left) and open (B, right) homology models of human Hv1 (Li et al., 2015) were superimposed using the Matchmaker program in Chimera (resource for Biocomputing, Visualization, and Informatics, University of California, San Francisco, San Francisco, CA; supported by NIGMS P41-GM103311; Pettersen et al., 2004) and are shown at the same viewing angle. S1, S2, S3, and S4 helices are indicated as red, yellow, green, and blue ribbons, respectively. The hydrophobic gasket residues V109 (on S1), F150 (on S2), and V177 and V178 (on S3) are indicated in brown.

row B is at  $pH_o$  7, and in both the effects of  $Zn^{2+}$  are profound. Drastic effects are already apparent at  $1 \mu M$   $Zn^{2+}$ : decreased current amplitude, a massive slowing of apparent activation, and a positive shift of the  $g_H$ -V relationship indicated by activation occurring at higher voltages. Surprisingly, however, the currents at  $10 \mu M$  or  $100 \mu M$   $Zn^{2+}$  appear kinetically similar to those at  $1 \mu M$   $Zn^{2+}$  and seem to differ mainly in their  $g_H$ -V relationships being shifted more positively. In WT proton channels,  $Zn^{2+}$  and other divalent metal cations slow activation

profoundly, but this effect increases distinctly with higher concentrations (Barish and Baud, 1984; Byerly et al., 1984; Mahaut-Smith, 1989a; Kapus et al., 1993; Cherny and DeCoursey, 1999; Musset et al., 2010b; Chaves et al., 2020). The slowing of activation by divalent metal cations in WT channels is greater than can be accounted for by the positive shift of the  $g_H$ -V relationship (Byerly et al., 1984; Kapus et al., 1993; Cherny and DeCoursey, 1999; Chaves et al., 2020). The phenomenology of  $Zn^{2+}$  interaction with the V116H monomer thus differs drastically from  $Zn^{2+}$  effects on WT channels. Fig. 9, C and D shows that the activation of this construct is quite rapid ( $\tau_{act}$  ranges from 200 to 300 ms at both  $pH_o$  6 and  $pH_o$  7) and is nearly independent of voltage. In WT Hv1 channels,  $\tau_{act}$  becomes distinctly faster at higher voltages, both in the absence or presence of  $Zn^{2+}$  or other divalent metals (Barish and Baud, 1984; Byerly et al., 1984; Mahaut-Smith, 1989a; Kapus et al., 1993; Cherny and DeCoursey, 1999; Chaves et al., 2020). There is a suggestion in the V116H data that  $\tau_{act}$  in the presence of  $Zn^{2+}$  actually slows at large positive voltages. Most surprisingly, the kinetics appears identical at all  $[Zn^{2+}]$ . In summary, in the V116H monomer, the activation kinetics in  $Zn^{2+}$  appears to be nearly independent of voltage,  $pH_o$ , and  $Zn^{2+}$  concentration.

The slowing of activation by divalent metals in WT Hv1 channels has been ascribed to the metals inhibiting channel opening (Cherny and DeCoursey, 1999; Qiu et al., 2016), and the

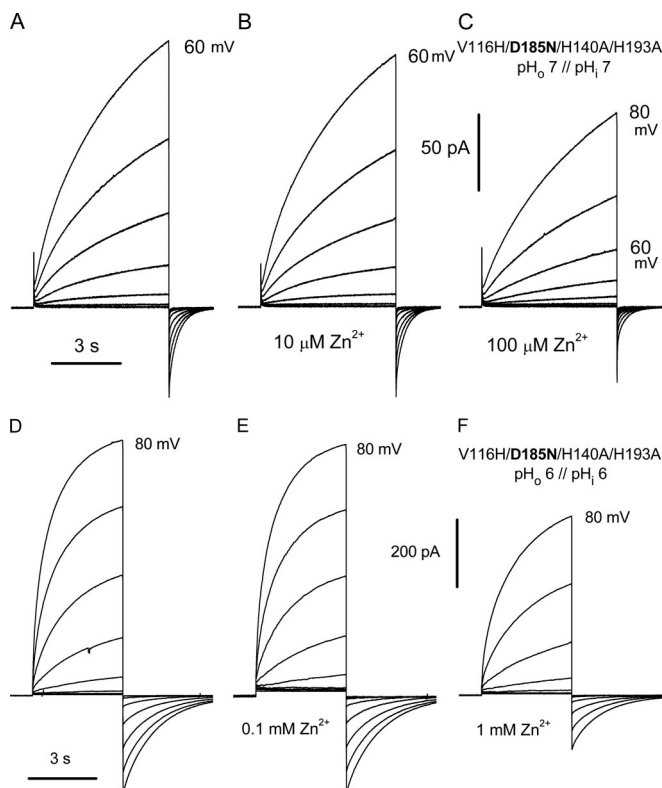


**Figure 6. Addition of the D185N mutation eliminates the  $Zn^{2+}$  sensitivity of V116H in the H140A/H193A background.** (A–C) A cell at  $pH_o$  7,  $pH_i$  7 is distinctly inhibited by  $100 \mu M$   $Zn^{2+}$ . Families were generated by pulses from  $V_{hold} = -40$  mV in 10-mV increments from  $-10$  mV up to the voltage indicated. (D–F) A different cell at  $pH_o$  6,  $pH_i$  6 is inhibited only at  $1 mM$   $Zn^{2+}$ . Families were generated by pulses from  $V_{hold} = -40$  mV in 10-mV increments from  $0$  mV up to  $+80$  mV.

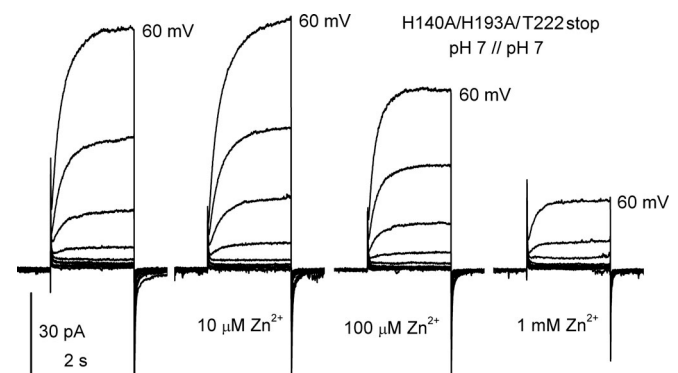


**Figure 7. The monomeric construct is insensitive to  $Zn^{2+}$ .**  $Zn^{2+}$  exerted minimal effects on the background construct used in this study, in which the two His that bind  $Zn^{2+}$  in WT channels were replaced with Ala, and the C terminus was truncated at position T222 (so that the final amino acid was K221).

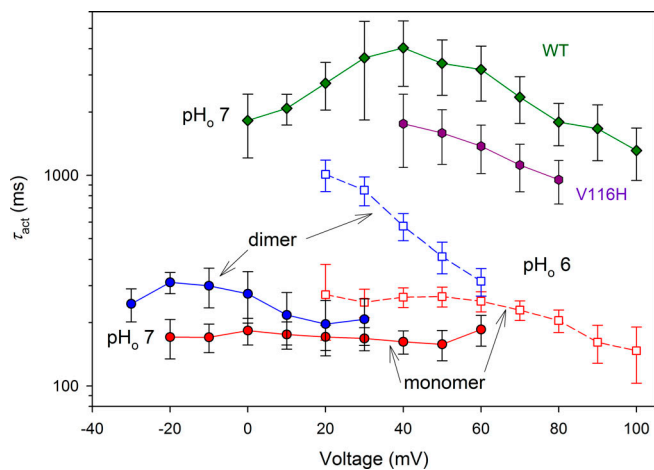
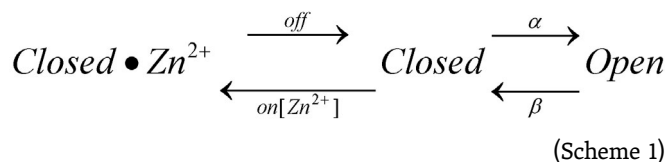


**Figure 8. Activation kinetics in the absence of  $\text{Zn}^{2+}$  in V116H/H140A/H193A constructs used here.** Values for  $\tau_{\text{act}}$  (mean  $\pm$  SEM) are plotted for dimeric (blue) and monomeric (red) V116H mutants at pH<sub>o</sub> 7 (solid symbols and lines) and pH<sub>o</sub> 6 (open symbols and dashed lines), all with pH<sub>i</sub> 6. For comparison,  $\tau_{\text{act}}$  from WT hH<sub>v</sub>1 is plotted (green) at pH<sub>o</sub> 7, pH<sub>i</sub> 7 (from Cherny et al., 2015), as well as the single mutant V116H at pH<sub>o</sub> 7 and pH<sub>i</sub> 7 (purple hexagons). It should be noted that  $\tau_{\text{act}}$  with pH<sub>i</sub> 7 is substantially slower than with pH<sub>i</sub> 6. Numbers of cells starting at the most negative voltage are WT 3, 3, 6, 9, 11, 12, 12, 12, 12, 8, and 6; pH<sub>o</sub> 7 dimer 3, 4, 4, 4, 4, 4, and 3; pH<sub>o</sub> 6 dimer 4, 4, 4, 4, and 4; pH<sub>o</sub> 7 monomer 5, 8, 9, 10, 10, 10, 10, 7, and 3; and pH<sub>o</sub> 6 monomer 3, 3, 14, 15, 15, 13, 4, and 3.

concentration-dependent effects on both kinetics and on the position of the  $g_{\text{H}}-V$  relationship can be described quantitatively by assuming the channel cannot open while bound by  $\text{Zn}^{2+}$  (Cherny and DeCoursey, 1999). The extraordinary concentration independence of  $\text{Zn}^{2+}$  effects on kinetics in the V116H monomer appears to indicate a different mechanism and is reminiscent of the concentration independence of the unbinding of drugs from their receptors. If the slow apparent activation in the presence of  $\text{Zn}^{2+}$  reflects the kinetics of  $\text{Zn}^{2+}$  unbinding from hH<sub>v</sub>1, this implies that the affinity of the closed state is much higher than that of the open state. In other words, channel opening lowers the affinity of the channel for  $\text{Zn}^{2+}$ , resulting in its release. The following simple model describes this phenomenon (Scheme 1):



From Fig. 9, C and D, it is evident that the unbinding rate ( $\text{off} \approx 1/\tau_{\text{act}}$ ) for  $\text{Zn}^{2+}$  from closed channels is low ( $0.1\text{--}0.5\text{ s}^{-1}$ ), whereas the opening rate ( $\alpha \approx 1/\tau_{\text{act}}$ ) is faster by an order of magnitude or more. Consequently, the  $\text{Closed} \bullet \text{Zn}^{2+} \rightarrow \text{Open}$  transition will be dominated by the unbinding rate ( $\text{off}$ ). We therefore designed experiments to test whether  $\text{Zn}^{2+}$  binding to the V116H monomer is state dependent, as portrayed in Scheme 1.

It was sometimes possible to discern transitions between the three states of Scheme 1 at low  $\text{Zn}^{2+}$  concentrations. Fig. 10, A and B shows families of currents at 0.1 and 10  $\mu\text{M}$   $\text{Zn}^{2+}$ ,

respectively. At the lower concentration, there clearly are rapid as well as slow components of current increase during depolarizing pulses. At the higher concentration, the slow component dominates (as it does throughout Fig. 9). Superimposing the currents at +90 mV in this experiment (Fig. 10 C) shows that the rapid component disappears at higher  $\text{Zn}^{2+}$  concentrations. We interpret the rapid component as the “normal” opening process of closed channels that do not have  $\text{Zn}^{2+}$  bound to them. At higher  $[\text{Zn}^{2+}]$ , essentially all (closed) channels have  $\text{Zn}^{2+}$  bound at the holding potential ( $V_{\text{hold}}$ ) and thus only the slowly rising current reflecting unbinding kinetics is observed.

#### **$\text{Zn}^{2+}$ binding to V116H channels exhibits state dependence**

Does  $\tau_{\text{act}}$  actually reflect  $\text{Zn}^{2+}$  unbinding kinetics? We will assume that  $\text{Zn}^{2+}$  binds to the closed monomeric channel, where it either occludes the conduction pathway or prevents opening. In Fig. 11, A and B, we applied a depolarizing pulse to remove  $\text{Zn}^{2+}$  from many channels, with the rising current reflecting the appearance of channels that are  $\text{Zn}^{2+}$  free and open. The entire current during this first pulse rose slowly, indicating that before the pulse all channels were closed and  $\text{Zn}^{2+}$  bound. Then we repolarized for variable times during which the channels should close and gradually bind  $\text{Zn}^{2+}$  again due to its high affinity for closed channels. If we apply a second depolarizing pulse after a short interval, the current should reflect a mixture of (1) channels still open, (2) channels that have closed but are still free of  $\text{Zn}^{2+}$ , and (3) channels that have closed and rebound  $\text{Zn}^{2+}$ . The time course of channel closing is evident directly from the tail current upon repolarization. During the subsequent depolarization, still-open channels will give rise to an instantaneous jump in current. Channels that are closed but  $\text{Zn}^{2+}$  free should open at the rapid rate characteristic of V116H channels in the absence of  $\text{Zn}^{2+}$  (Fig. 9). Finally, those channels that closed and rebound  $\text{Zn}^{2+}$  during the interval should produce a slowly activating component as the opening process expels  $\text{Zn}^{2+}$  from the channel.

Fig. 11 shows experiments done to determine whether these three components exist and are occupied according to Scheme 1. In Fig. 11, A and B, a pair of pulses to +60 mV was applied with a variable interval between them. The current elicited by the first pulse rose slowly. In contrast, during the second pulse applied after a short interval, there was an instantaneous jump (channels still open), followed by a rapidly rising component ( $\text{Closed} \rightarrow \text{Open}$ ), and finally a slowly rising phase ( $\text{Closed} \bullet \text{Zn}^{2+} \rightarrow \text{Open}$ ). During the second pulse, channels that were still open remained open, producing an instantaneous jump on depolarization. Channels that closed but were not yet blocked by  $\text{Zn}^{2+}$  during the interval should open with the same rapid time course seen in the absence of  $\text{Zn}^{2+}$  (●; Fig. 9, C and D). As the tail current abates, the instantaneous jump decreases in amplitude, with a generally similar time course. In addition, the rapidly rising component becomes smaller as more channels become blocked ( $\text{Closed} \rightarrow \text{Closed} \bullet \text{Zn}^{2+}$ ) at  $V_{\text{hold}}$ . The disappearance of the rapidly rising component should reflect the rate of  $\text{Zn}^{2+}$  binding to closed channels at  $V_{\text{hold}}$  (although they must close before becoming blocked). Channels that close and bind  $\text{Zn}^{2+}$  again should reopen with the slow time course that reflects  $\text{Zn}^{2+}$  unbinding



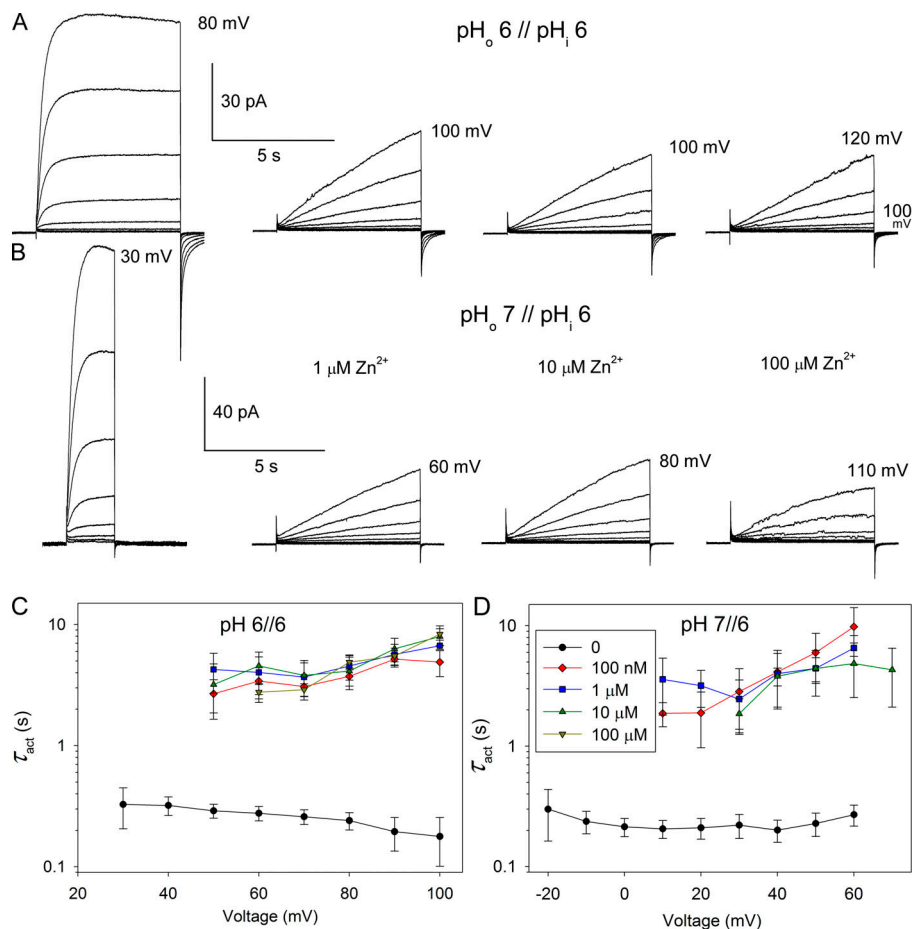


**Figure 9. In the V116H monomer, the turn-on of current in the presence of  $Zn^{2+}$  is practically independent of both voltage and  $Zn^{2+}$  concentration. (A and B)** Families of currents are shown at pH<sub>o</sub> 6 (A) and pH<sub>o</sub> 7 (B), both with pH<sub>i</sub> 6, in the indicated concentrations of  $Zn^{2+}$  with pulses applied in 10-mV increments up to the voltage shown. **(C and D)** The  $\tau_{act}$  values (mean  $\pm$  SEM) from these cells are shown in the absence (●) or presence of  $Zn^{2+}$  in concentrations indicated in the inset to D. Every  $\tau_{act}$  value at every voltage is significantly ( $P < 0.05$ ) higher in  $Zn^{2+}$  than in control in C and D except two values at +60 mV in D. Numbers of cells at pH<sub>o</sub> 6 are control 3–10, 100 nM  $Zn^{2+}$  2–7, 1  $\mu$ M  $Zn^{2+}$  2–8, 10  $\mu$ M  $Zn^{2+}$  3–6, and 100  $\mu$ M  $Zn^{2+}$  3–5; numbers of cells at pH<sub>o</sub> 7 are control 3–7, 100 nM  $Zn^{2+}$  2 or 3, 1  $\mu$ M  $Zn^{2+}$  2–4, and 10  $\mu$ M  $Zn^{2+}$  3. The control values are a subset of those plotted in Fig. 8; here, we include only cells in which we also had  $\tau_{act}$  data in  $Zn^{2+}$ .

kinetics. The three predicted components during the second pulse are all evident in Fig. 11. After a long interval at  $-60$  mV, all the channels reopened with a slow time course, essentially identical to the current seen during the first pulse (Fig. 11 A). After short intervals, both an instantaneous jump and then an initial rapid rising phase can be seen.

If this interpretation is correct, one might predict that if the voltage during the interpulse interval differs from  $V_{hold}$ , the rate at which these transitions occur should change. In Fig. 11 B, we tested this by stepping to  $0$  mV during the interpulse interval. The tail current was now outward and decayed more slowly than it did at  $-60$  mV in Fig. 11 A. The envelope of instantaneous current jumps during the depolarizing pulses was clearly slower

than in Fig. 11 A. The presence of a distinct rapidly rising component also was visible after longer intervals than in Fig. 11 A.

Another prediction of Scheme 1 is that if the rapidly rising component reflects channels that were unblocked and opened by the preceding pulse, then if the first pulse is short, only a few channels will have had the opportunity to become unblocked. Therefore, as we lengthen the first pulse, more channels should open and become unblocked and the rapid component should increase in amplitude. Fig. 11 C illustrates this kind of experiment. The second pulse following a brief depolarization exhibited almost no fast component but had a larger instantaneous jump because repolarization was too brief for all the open channels to close. As the first pulse became longer, the rapidly

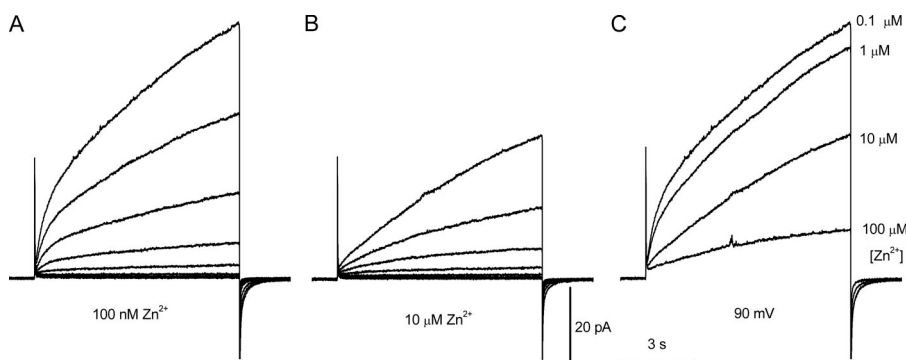


**Figure 10. Families of currents in the V116H monomer at pH 6/6. (A and B)** Pulses are in 10-mV increments from  $V_{hold} = -40$  mV to  $+90$  mV. Note that there is a distinct rapidly rising phase in A at 100 nM  $Zn^{2+}$  but not in B at 10  $\mu$ M  $Zn^{2+}$ . **(C)** In the same cell, currents at  $+90$  mV are superimposed in the presence of the indicated  $Zn^{2+}$ . The fast component is only detectable at low  $[Zn^{2+}]$ .

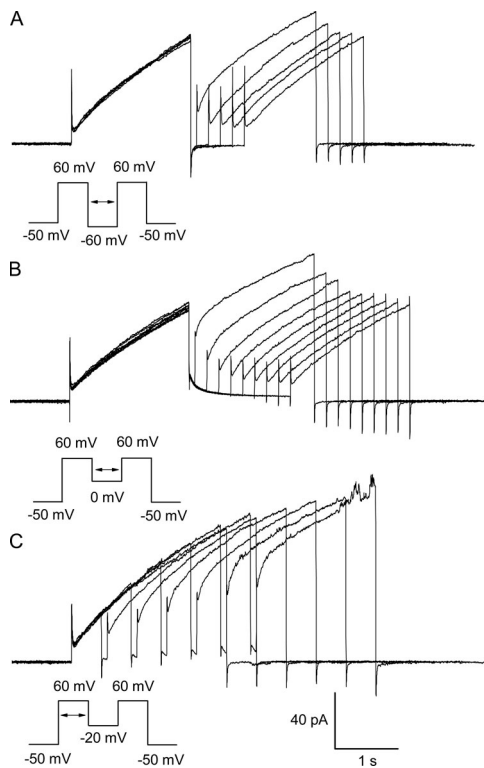


Figure 11. Pulse pair experiments in the V116H monomer (V116H/H140A/H193A/T222stop) reveal two components of “activation.” (A and B) Panels differ only in the interpulse voltages of  $-60$  mV or  $0$  mV, respectively. (C) The first pulse duration was varied. All measurements were from a cell at  $\text{pH}_o$  7,  $\text{pH}_i$  6 with  $1 \mu\text{M}$   $\text{Zn}^{2+}$ .

rising component increased in amplitude, as did the instantaneous jump. In all experiments in Fig. 11, fitting the current during the second pulse with two exponentials revealed that the two time constants remained constant, but their amplitudes varied. In a number of similar measurements, the fast and slow time constants extracted were variable but usually were reasonably close to  $\tau_{\text{act}}$  in the absence of  $\text{Zn}^{2+}$  and  $\tau_{\text{act}}$  in the presence of  $\text{Zn}^{2+}$ , respectively. For example, in the cell in Fig. 11, in the absence of  $\text{Zn}^{2+}$  at  $\text{pH}_o$  7,  $\tau_{\text{act}}$  was independent of voltage and averaged 236 ms, and the fast component  $\tau_{\text{act}}$  in  $1 \mu\text{M}$   $\text{Zn}^{2+}$  in Fig. 11 B ranged from 78 to 317 ms. For the first pulse in Fig. 11 B,  $\tau_{\text{act}}$  was  $3.1 \pm 0.71$  s ( $n = 11$ ), and the slower component in double exponential fits of the second pulse was  $3.4 \pm 0.36$  s ( $n = 10$ ;  $P = 0.24$ ).

## Discussion

The phenomenology of  $\text{Zn}^{2+}$  effects on V116H and WT  $\text{H}_v1$  channels is strikingly different. In WT channels, it was possible to explain the slowing of activation and the shift of the  $g_{\text{H}}-V$  relationship by making a single assumption, that the channel cannot open with  $\text{Zn}^{2+}$  bound (Cherny and DeCoursey, 1999). The measured macroscopic rate of opening depends directly on the fraction of channels that have no  $\text{Zn}^{2+}$  bound. For example, at the  $K_d$  for  $\text{Zn}^{2+}$  binding, 50% of the channels are  $\text{Zn}^{2+}$  bound and  $\tau_{\text{act}}$  is accordingly twice slower. If the opening rate is slowed

but the closing rate is not affected, the  $g_{\text{H}}-V$  relationship shifts positively. These relationships do not hold for the V116H mutant. The decrease in current amplitude was much more pronounced than in WT  $\text{hH}_v1$ . The most remarkable phenomenon occurred in monomeric constructs. Because activation of monomeric  $\text{H}_v1$  is much faster than of dimeric channels (Koch et al., 2008; Tombola et al., 2008; Musset et al., 2010b; Fujiwara et al., 2013), two components could be distinguished. At very low  $[\text{Zn}^{2+}]$ , a rapid component with a time constant like that in the absence of  $\text{Zn}^{2+}$  was observed, together with a very slow component ( $\tau$  was 2–10 s; Fig. 9). At  $1 \mu\text{M}$  or higher  $[\text{Zn}^{2+}]$ , the current generally turned on with a single slow time constant that was independent of both  $\text{Zn}^{2+}$  concentration and voltage. The simplest explanation is provided by analogy with drug–receptor interactions in which drug unbinding is independent of concentration. “Block” of V116H is purely state dependent, with extremely high-affinity binding to closed channels and essentially no affinity for open channels. In this view,  $\text{Zn}^{2+}$  affinity is so high that for  $1 \mu\text{M}$  or higher  $[\text{Zn}^{2+}]$ , essentially all channels in a closed state have  $\text{Zn}^{2+}$  attached.  $\text{Zn}^{2+}$  unbinding allows rearrangement of the protein that results in channel opening. The different phenomenology of WT and V116H channels evidently results mainly from the slow off rate for  $\text{Zn}^{2+}$  in V116H channels.

The combination of rapid activation kinetics of the monomeric construct combined with the slow off rate of  $\text{Zn}^{2+}$  made it possible to detect two clear components of turn-on of current in the presence of  $\text{Zn}^{2+}$ . Several kinds of data support the interpretation that the rapid opening in the presence of  $\text{Zn}^{2+}$  reflects normal opening kinetics of the mutant channels. The slower component appears to reflect the rate of  $\text{Zn}^{2+}$  unbinding as channels open. Like drug dissociation kinetics,  $\text{Zn}^{2+}$  dissociation occurs at the same rate independently of  $\text{Zn}^{2+}$  concentration. Fitting with two exponentials produces two time constants that are close to those of activation of the V116H channel in the absence of  $\text{Zn}^{2+}$  and the slow component that dominates at high  $\text{Zn}^{2+}$  concentrations. Varying pulse durations produce changes in the amplitudes of fast and slow components that are consistent with expectations of Scheme 1. The simple model in Scheme 1 can occur only if the affinity of the channel for  $\text{Zn}^{2+}$  is much lower when the channel opens. The present evidence strongly indicates that  $\text{Zn}^{2+}$  binds almost exclusively to closed V116H channels.

## What explains the extraordinarily high affinity of $\text{Zn}^{2+}$ binding to V116H?

The affinity of  $\text{Zn}^{2+}$  for His in solution is rather weak;  $K_d$  is  $322 \mu\text{M}$  at  $\text{pH}$  7.4,  $25^\circ\text{C}$ , and  $0.1$  M ionic strength (Krežel and Maret, 2016). Higher-affinity  $\text{Zn}^{2+}$  binding to catalytic sites in proteins typically results from tetrahedral coordination by liganding groups, usually His, Glu, Asp, or Cys and water (Alberts et al., 1998; Auld, 2001). The native  $\text{Zn}^{2+}$  binding site in  $\text{hH}_v1$  and  $\text{mH}_v1$  comprises two His (His<sup>140</sup> and His<sup>193</sup> in  $\text{hH}_v1$ ; Ramsey et al., 2006; Musset et al., 2010b) with minor contributions from E119 and D123 (in  $\text{mH}_v1$  with  $\text{hH}_v1$  numbering; Takeshita et al., 2014). Some studies concluded that these residues produced two distinct metal binding sites in several species (Qiu et al., 2016; Chaves et al., 2020; Jardin et al., 2020). Although



native H<sub>v</sub>1 channels from mammalian species are clearly inhibited by 1 or even 0.1  $\mu$ M Zn<sup>2+</sup> (Cherny and DeCoursey, 1999; Lishko et al., 2010), distinct effects on the single His at position 116 were observed at 10 nM Zn<sup>2+</sup> (Fig. 2 B). Quantified by the decrease of current, Zn<sup>2+</sup> is at least two orders of magnitude more potent for V116H than for WT channels (Fig. 4).

The potent Zn<sup>2+</sup> binding suggests that other coordinating groups participate. Position 116 in the closed channel model of hH<sub>v</sub>1 is reasonably near three acidic groups (D112, E119, and D185) that are potential candidates. Position 116 is between D112 and E119 vertically but is directly across from D185 (Fig. 5). The negativity of Asp<sup>185</sup> would be expected to strongly enhance Zn<sup>2+</sup> affinity (Gurd and Wilcox, 1956). To test whether Asp<sup>185</sup> does indeed contribute, we replaced it with Asn, D185N. Fig. 6 shows that replacing Asp<sup>185</sup> with Asn abolished high-affinity Zn<sup>2+</sup> binding to His<sup>116</sup>. We conclude from the high-affinity Zn<sup>2+</sup> binding to His<sup>116</sup> in the presence of Asp<sup>185</sup> that these two positions are at a similar height in the closed channel.

### State-dependent Zn<sup>2+</sup> binding to His<sup>116</sup> and Asp<sup>185</sup> defines interactions in closed and open hH<sub>v</sub>1 channels

Despite a crystal structure (Takeshita et al., 2014), electron paramagnetic resonance measurements (Li et al., 2015), and a profusion of homology models and MD simulations (Musset et al., 2010b; Ramsey et al., 2010; Wood et al., 2012; Kulleperuma et al., 2013; Morgan et al., 2013; Chamberlin et al., 2014, 2015; Pupo et al., 2014; Gianti et al., 2016; Qiu et al., 2016; Randolph et al., 2016; van Keulen et al., 2017; Banh et al., 2019; Jardin et al., 2020), there is little certainty with respect to closed or open structures or the molecular rearrangements that occur during gating. Depolarization of V116H presumably rearranges the channel protein, drastically lowering Zn<sup>2+</sup> affinity. As Zn<sup>2+</sup> unbinds, current appears. What drives Zn<sup>2+</sup> unbinding? Is the binding site within the electric field? If this were the case, greater depolarization would remove Zn<sup>2+</sup> faster and more completely. Contradicting this proposal,  $\tau_{act}$  appears roughly independent of voltage in the presence of Zn<sup>2+</sup> or perhaps even slows at increasingly positive voltages. However, because Zn<sup>2+</sup> unbinding (off) is much slower than channel opening ( $\alpha$ ), any voltage dependence could be masked. We conclude that Zn<sup>2+</sup> simply has a much lower affinity in the open state.

An explanation for state-dependent Zn<sup>2+</sup> binding is suggested by comparing closed and open hH<sub>v</sub>1 models based on electron paramagnetic resonance measurements of hH<sub>v</sub>1 (Li et al., 2015) and informed by crystal structures of “down” and “up” (representing hyperpolarized and depolarized configurations, respectively) of the CiVSP (*Ciona intestinalis* voltage sensing phosphatase; Li et al., 2014). In the closed state, R1 (Arg<sup>205</sup> in hH<sub>v</sub>1) interacts with Asp<sup>112</sup>, leaving sidechains at position 116 and Asp<sup>185</sup> available for interaction. This interaction is supported by the crystal structure of closed mH<sub>v</sub>1 (Takeshita et al., 2014). To reach the open state, the protein rearranges (DeCoursey, 2015a; Li et al., 2015) such that Asp<sup>112</sup> can interact with Arg<sup>208</sup> (Kulleperuma et al., 2013; Li et al., 2015), forming the selectivity filter (Musset et al., 2011). This rearrangement also inserts Arg<sup>205</sup> directly between sidechains at position 116 and Asp<sup>185</sup>. The intrusion of cationic Arg<sup>205</sup> in the middle of the

Zn<sup>2+</sup>-binding site would repel Zn<sup>2+</sup> electrostatically. This intuitive view suggests that as the channel begins its opening transition, as a result of the conformational change Arg<sup>205</sup> repels the Zn<sup>2+</sup>. Any voltage dependence that might be expected is overshadowed by the high affinity of binding, such that the slow off rate in Scheme 1 dominates.

MD simulations by Qiu et al. (2016) predict two Zn<sup>2+</sup> binding sites in CiH<sub>v</sub>1. The deeper site (from the outside) corresponding to Asp<sup>112</sup> and Asp<sup>185</sup> in hH<sub>v</sub>1 was predicted to be more accessible to Zn<sup>2+</sup> in the closed state. This is generally consistent with the experimental evidence presented here, and we demonstrate that, in all likelihood, in V116H Zn<sup>2+</sup> is coordinated by the introduced His<sup>116</sup> and by Asp<sup>185</sup>. In the Li model of closed hH<sub>v</sub>1, positions 116 and 185 are directly across the pore from each other (Li et al., 2015). In contrast, in the crystal structure of the closed mH<sub>v</sub>1 (Takeshita et al., 2014), Asp<sup>185</sup> is distinctly lower than position 116 (both human numbering). To date, no crystal structure exists of the entire H<sub>v</sub>1 protein from any species, perhaps due to its high protein mobility (Li et al., 2015). The existing crystal structure is a chimera of mouse H<sub>v</sub>1, with its N terminus truncated, its C terminus replaced by a leucine-zipper motif of the transcriptional activator GCN4 from *Saccharomyces cerevisiae*, and with a section of *C. intestinalis* voltage-sensing phosphatase spliced in from the middle of S2 to the middle of S3. It has been suggested that insertion of the CiVSP peptide at the inner side of S2-S3 resulted in S3 in the crystal structure being too low by one helical turn (DeCoursey, 2015a; Li et al., 2015; Banh et al., 2019). Thus, the high-affinity Zn<sup>2+</sup> binding observed here between V116H and D185 supports the Li et al. closed state model.

In summary, the Zn<sup>2+</sup> sensitivity of the V116H mutant strongly suggests that the closed model of hH<sub>v</sub>1 proposed by Li et al. (2015) more closely reflects the closed channel structure than does the crystal structure of mH<sub>v</sub>1 (Takeshita et al., 2014), specifically in the region including the inner ends of the S2 and S3 helices. In the closed state, position 116 is directly across the pore from Asp<sup>185</sup>; and these two positions in the V116H mutant form an extremely high-affinity binding site for Zn<sup>2+</sup>. These relationships exist in a closed state near the open state, but it is possible that deeper closed states exist. The most straightforward explanation for the loss of Zn<sup>2+</sup> affinity in open channels is that repositioning of S4 brings Arg<sup>205</sup> between His<sup>116</sup> and Asp<sup>185</sup>, expelling Zn<sup>2+</sup> electrostatically. Our open state model requires no further movement of S4, but based on the present data, we cannot rule out the possibility that S4 might proceed farther. However, R211H mutants are inhibited by internally applied Zn<sup>2+</sup>, supporting the idea that in the open state Asp<sup>112</sup> interacts with Arg<sup>208</sup> (Kulleperuma et al., 2013; Morgan et al., 2013). It is difficult to escape the conclusion that during opening, hH<sub>v</sub>1 at a minimum traverses the two experimentally defined positions depicted in Fig. 5.

The relatively small excursion of S4 in closed and open states resolved here may appear to contradict the gating charge estimated for H<sub>v</sub>1 by measurements of the limiting slope of the  $g_H$ -V relationship (Almers, 1978). For native (DeCoursey and Cherny, 1996, 1997) and WT dimeric channels (Musset et al., 2008; Fujiwara et al., 2012; Gonzalez et al., 2013; Thomas et al., 2018),

the gating charge tends toward the higher end of 4–6  $e_0$ . For monomeric constructs,  $e_0$  is half that (Gonzalez et al., 2010; Fujiwara et al., 2012; Gonzalez et al., 2013). If one assumes that the gating charge reflects the charge of all three Arg from S4 moving across the entire membrane electrical field, the smaller movement implied by the present results would appear to produce too little charge movement. However, charges in proteins other than Arg may contribute; for example, anionic charges on S1 may move inward (Mony et al., 2015). More importantly, gating current can result from obligatory protonation of internal acidic groups and deprotonation of external ones. This mechanism was proposed in a model that explained quantitatively the mechanism of  $\Delta$ pH-dependent gating (Cherny et al., 1995), the establishment of the position of the  $g_{H^+}$ -V relationship by the pH gradient ( $\Delta$ pH =  $pH_o - pH_i$ ). An updated, but less quantitative version of this idea was proposed recently (the “counter-charge model”) that emphasized the natural way in which the breaking and forming of salt bridges within the channel protein stabilizes closed and open states in a manner consistent with its producing  $\Delta$ pH-dependent gating (DeCoursey, 2018). Protonation/deprotonation of sites within the membrane electrical field is practically indistinguishable from the gating charge resulting from the more traditional movement of charged groups within the protein.

## Acknowledgments

Christopher J. Lingle served as editor.

This work was supported by National Institutes of Health grant R35 GM126902 (to T.E. DeCoursey), Deutsche Forschungsgemeinschaft grant MU 3574/4-1 (to B. Musset), and Bears Care (to D. Morgan). The content is solely the responsibility of the authors and does not necessarily represent the official views of the National Institutes of Health.

The authors declare no competing financial interests.

Author contributions: S.M.E. Smith and T.E. DeCoursey conceptualized the study. T.E. DeCoursey interpreted the data. V.V. Cherny, D. Morgan, B. Musset, and T.E. DeCoursey conducted experiments and performed the data analysis. T.E. DeCoursey, D. Morgan, and B. Musset acquired the funding. S.M.E. Smith and T.E. DeCoursey administered the project. S. Thomas and S.M.E. Smith provided resources. T.E. DeCoursey wrote the original draft of the manuscript. All authors reviewed and approved the manuscript.

Submitted: 19 May 2020

Accepted: 10 August 2020

## References

Alberts, I.L., K. Nadassy, and S.J. Wodak. 1998. Analysis of zinc binding sites in protein crystal structures. *Protein Sci.* 7:1700–1716. <https://doi.org/10.1002/pro.5560070805>

Almers, W. 1978. Gating currents and charge movements in excitable membranes. *Rev. Physiol. Biochem. Pharmacol.* 82:96–190. <https://doi.org/10.1007/BFb0030498>

Auld, D.S. 2001. Zinc coordination sphere in biochemical zinc sites. *Biomaterials.* 14:271–313. <https://doi.org/10.1023/A:1012976615056>

Banh, R., V.V. Cherny, D. Morgan, B. Musset, S. Thomas, K. Kulleperuma, S.M.E. Smith, R. Pomès, and T.E. DeCoursey. 2019. Hydrophobic gasket

mutation produces gating pore currents in closed human voltage-gated proton channels. *Proc. Natl. Acad. Sci. USA.* 116:18951–18961. <https://doi.org/10.1073/pnas.1905462116>

Barish, M.E., and C. Baud. 1984. A voltage-gated hydrogen ion current in the oocyte membrane of the axolotl, *Ambystoma*. *J. Physiol.* 352:243–263. <https://doi.org/10.1113/jphysiol.1984.sp015289>

Bers, D. 2009. WEBMAXC STANDARD. University of California, Davis. <https://somapp.ucdmc.ucdavis.edu/pharmacology/bers/maxchelator/webmaxc/webmaxcS.htm> (accessed June 2019)

Byerly, L., R. Meech, and W. Moody, Jr. 1984. Rapidly activating hydrogen ion currents in perfused neurones of the snail, *Lymnaea stagnalis*. *J. Physiol.* 351:199–216. <https://doi.org/10.1113/jphysiol.1984.sp015241>

Chamberlin, A., F. Qiu, S. Rebolledo, Y. Wang, S.Y. Noskov, and H.P. Larsson. 2014. Hydrophobic plug functions as a gate in voltage-gated proton channels. *Proc. Natl. Acad. Sci. USA.* 111:E273–E282. <https://doi.org/10.1073/pnas.1318018111>

Chamberlin, A., F. Qiu, Y. Wang, S.Y. Noskov, and H.P. Larsson. 2015. Mapping the gating and permeation pathways in the voltage-gated proton channel Hv1. *J. Mol. Biol.* 427:131–145. <https://doi.org/10.1016/j.jmb.2014.11.018>

Chaves, G., S. Bungert-Plümke, A. Franzen, I. Mahorivska, and B. Musset. 2020. Zinc modulation of proton currents in a new voltage-gated proton channel suggests a mechanism of inhibition. *FEBS J.* febs.15291. <https://doi.org/10.1111/febs.15291>

Cherny, V.V., and T.E. DeCoursey. 1999. pH-dependent inhibition of voltage-gated  $H^+$  currents in rat alveolar epithelial cells by  $Zn^{2+}$  and other divalent cations. *J. Gen. Physiol.* 114:819–838. <https://doi.org/10.1085/jgp.114.6.819>

Cherny, V.V., V.S. Markin, and T.E. DeCoursey. 1995. The voltage-activated hydrogen ion conductance in rat alveolar epithelial cells is determined by the pH gradient. *J. Gen. Physiol.* 105:861–896. <https://doi.org/10.1085/jgp.105.6.861>

Cherny, V.V., D. Morgan, B. Musset, G. Chaves, S.M.E. Smith, and T.E. DeCoursey. 2015. Tryptophan 207 is crucial to the unique properties of the human voltage-gated proton channel, hHv1. *J. Gen. Physiol.* 146:343–356. <https://doi.org/10.1085/jgp.201511456>

DeCoursey, T.E. 2003. Voltage-gated proton channels and other proton transfer pathways. *Physiol. Rev.* 83:475–579. <https://doi.org/10.1152/physrev.00028.2002>

DeCoursey, T.E. 2013. Voltage-gated proton channels: molecular biology, physiology, and pathophysiology of the  $H_v$  family. *Physiol. Rev.* 93: 599–652. <https://doi.org/10.1152/physrev.00011.2012>

DeCoursey, Thomas E. 2015a. Structural revelations of the human proton channel. *Proc. Natl. Acad. Sci. USA.* 112:13430–13431. <https://doi.org/10.1073/pnas.1518486112>

DeCoursey, T.E. 2018. Voltage and pH sensing by the voltage-gated proton channel,  $H_v1$ . *J. R. Soc. Interface.* 15. 20180108. <https://doi.org/10.1098/rsif.2018.0108>

DeCoursey, Thomas E. 2015b. The Voltage-Gated Proton Channel: A Riddle, Wrapped in a Mystery, inside an Enigma. *Biochemistry.* 54:3250–3268. <https://doi.org/10.1021/acs.biochem.5b00353>

DeCoursey, T.E., and V.V. Cherny. 1996. Effects of buffer concentration on voltage-gated  $H^+$  currents: does diffusion limit the conductance? *Biophys. J.* 71:182–193. [https://doi.org/10.1016/S0006-3495\(96\)79215-9](https://doi.org/10.1016/S0006-3495(96)79215-9)

DeCoursey, T.E., and V.V. Cherny. 1997. Deuterium isotope effects on permeation and gating of proton channels in rat alveolar epithelium. *J. Gen. Physiol.* 109:415–434. <https://doi.org/10.1085/jgp.109.4.415>

DeCoursey, T.E., D. Morgan, B. Musset, and V.V. Cherny. 2016. Insights into the structure and function of  $H_v1$  from a meta-analysis of mutation studies. *J. Gen. Physiol.* 148:97–118. <https://doi.org/10.1085/jgp.201611619>

Eder, C., H.G. Fischer, U. Hadding, and U. Heinemann. 1995. Properties of voltage-gated currents of microglia developed using macrophage colony-stimulating factor. *Pflügers Arch.* 430:526–533. <https://doi.org/10.1007/BF00373889>

Fujiwara, Y., T. Kurokawa, K. Takeshita, M. Kobayashi, Y. Okochi, A. Nakagawa, and Y. Okamura. 2012. The cytoplasmic coiled-coil mediates cooperative gating temperature sensitivity in the voltage-gated  $H^+$  channel Hv1. *Nat. Commun.* 3:816. <https://doi.org/10.1038/ncomms1823>

Fujiwara, Y., T. Kurokawa, K. Takeshita, A. Nakagawa, H.P. Larsson, and Y. Okamura. 2013. Gating of the designed trimeric/tetrameric voltage-gated  $H^+$  channel. *J. Physiol.* 591:627–640. <https://doi.org/10.1113/jphysiol.2012.243006>

Fujiwara, Y., T. Kurokawa, and Y. Okamura. 2014. Long  $\alpha$  helices projecting from the membrane as the dimer interface in the voltage-gated  $H^+$  channel. *J. Gen. Physiol.* 143:377–386. <https://doi.org/10.1085/jgp.201311082>

- Gianti, E., L. Delemotte, M.L. Klein, and V. Carnevale. 2016. On the role of water density fluctuations in the inhibition of a proton channel. *Proc. Natl. Acad. Sci. USA*. 113:E8359–E8368. <https://doi.org/10.1073/pnas.1609964114>
- Gonzalez, C., H.P. Koch, B.M. Drum, and H.P. Larsson. 2010. Strong cooperativity between subunits in voltage-gated proton channels. *Nat. Struct. Mol. Biol.* 17:51–56. <https://doi.org/10.1038/nsmb.1739>
- Gonzalez, C., S. Rebolledo, M.E. Perez, and H.P. Larsson. 2013. Molecular mechanism of voltage sensing in voltage-gated proton channels. *J. Gen. Physiol.* 141:275–285. <https://doi.org/10.1085/jgp.201210857>
- Gurd, F.R., and P.E. Wilcox. 1956. Complex formation between metallic cations and proteins, peptides and amino acids. *Adv. Protein Chem.* 11: 311–427. [https://doi.org/10.1016/S0065-3233\(08\)60424-6](https://doi.org/10.1016/S0065-3233(08)60424-6)
- Jardin, C., G. Chaves, and B. Musset. 2020. Assessing structural determinants of Zn<sup>2+</sup> binding to human Hv1 via multiple MD simulations. *Biophys. J.* 118:1221–1233. <https://doi.org/10.1016/j.bpj.2019.12.035>
- Kapus, A., R. Romanek, A.Y. Qu, O.D. Rotstein, and S. Grinstein. 1993. A pH-sensitive and voltage-dependent proton conductance in the plasma membrane of macrophages. *J. Gen. Physiol.* 102:729–760. <https://doi.org/10.1085/jgp.102.4.729>
- Kariev, A.M., and M.E. Green. 2018. The role of proton transport in gating current in a voltage gated ion channel, as shown by quantum calculations. *Sensors (Basel)*. 18:3143. <https://doi.org/10.3390/s18093143>
- Koch, H.P., T. Kurokawa, Y. Okochi, M. Sasaki, Y. Okamura, and H.P. Larsson. 2008. Multimeric nature of voltage-gated proton channels. *Proc. Natl. Acad. Sci. USA*. 105:9111–9116. <https://doi.org/10.1073/pnas.0801553105>
- Krężel, A., and W. Maret. 2016. The biological inorganic chemistry of zinc ions. *Arch. Biochem. Biophys.* 611:3–19. <https://doi.org/10.1016/j.abb.2016.04.010>
- Kulleperuma, K., S.M.E. Smith, D. Morgan, B. Musset, J. Holyoake, N. Chakrabarti, V.V. Cherny, T.E. DeCoursey, and R. Pomès. 2013. Construction and validation of a homology model of the human voltage-gated proton channel hHv1. *J. Gen. Physiol.* 141:445–465. <https://doi.org/10.1085/jgp.201210856>
- Lee, C.H., and R. MacKinnon. 2019. Voltage sensor movements during hyperpolarization in the HCN channel. *Cell*. 179:1582–1589.e7. <https://doi.org/10.1016/j.cell.2019.11.006>
- Lee, S.Y., J.A. Letts, and R. MacKinnon. 2008. Dimeric subunit stoichiometry of the human voltage-dependent proton channel Hv1. *Proc. Natl. Acad. Sci. USA*. 105:7692–7695. <https://doi.org/10.1073/pnas.0803277105>
- Li, Q., S. Wanderling, M. Paduch, D. Medovoy, A. Singharoy, R. McGreevy, C.A. Villalba-Galea, R.E. Hulse, B. Roux, K. Schulten, et al. 2014. Structural mechanism of voltage-dependent gating in an isolated voltage-sensing domain. *Nat. Struct. Mol. Biol.* 21:244–252. <https://doi.org/10.1038/nsmb.2768>
- Li, Q., R. Shen, J.S. Tregger, S.S. Wanderling, W. Milewski, K. Siwowska, F. Bezanilla, and E. Perozo. 2015. Resting state of the human proton channel dimer in a lipid bilayer. *Proc. Natl. Acad. Sci. USA*. 112: E5926–E5935. <https://doi.org/10.1073/pnas.1515043112>
- Lishko, P.V., I.L. Botchkina, A. Fedorenko, and Y. Kirichok. 2010. Acid extrusion from human spermatozoa is mediated by flagellar voltage-gated proton channel. *Cell*. 140:327–337. <https://doi.org/10.1016/j.cell.2009.12.053>
- Mahaut-Smith, M.P. 1989a. The effect of zinc on calcium and hydrogen ion currents in intact snail neurones. *J. Exp. Biol.* 145:455–464.
- Mahaut-Smith, M.P. 1989b. Separation of hydrogen ion currents in intact molluscan neurones. *J. Exp. Biol.* 145:439–454.
- Mony, L., T.K. Berger, and E.Y. Isacoff. 2015. A specialized molecular motion opens the Hv1 voltage-gated proton channel. *Nat. Struct. Mol. Biol.* 22: 283–290. <https://doi.org/10.1038/nsmb.2978>
- Morgan, D., B. Musset, K. Kulleperuma, S.M.E. Smith, S. Rajan, V.V. Cherny, R. Pomès, and T.E. DeCoursey. 2013. Peregrination of the selectivity filter delineates the pore of the human voltage-gated proton channel hHv1. *J. Gen. Physiol.* 142:625–640. <https://doi.org/10.1085/jgp.201311045>
- Musset, B., V.V. Cherny, D. Morgan, Y. Okamura, I.S. Ramsey, D.E. Clapham, and T.E. DeCoursey. 2008. Detailed comparison of expressed and native voltage-gated proton channel currents. *J. Physiol.* 586:2477–2486. <https://doi.org/10.1113/jphysiol.2007.149427>
- Musset, B., S.M.E. Smith, S. Rajan, V.V. Cherny, D. Morgan, and T.E. DeCoursey. 2010a. Oligomerization of the voltage-gated proton channel. *Channels (Austin)*. 4:260–265. <https://doi.org/10.4161/chan.4.4.12789>
- Musset, B., S.M.E. Smith, S. Rajan, V.V. Cherny, S. Sujai, D. Morgan, and T.E. DeCoursey. 2010b. Zinc inhibition of monomeric and dimeric proton channels suggests cooperative gating. *J. Physiol.* 588:1435–1449. <https://doi.org/10.1113/jphysiol.2010.188318>
- Musset, B., S.M.E. Smith, S. Rajan, D. Morgan, V.V. Cherny, and T.E. DeCoursey. 2011. Aspartate112 is the selectivity filter of the human voltage-gated proton channel. *Nature*. 480:273–277. <https://doi.org/10.1038/nature10557>
- Paoletti, P., P. Ascher, and J. Neyton. 1997. High-affinity zinc inhibition of NMDA NR1-NR2A receptors. *J. Neurosci.* 17:5711–5725. <https://doi.org/10.1523/JNEUROSCI.17-15-05711.1997>
- Pettersen, E.F., T.D. Goddard, C.C. Huang, G.S. Couch, D.M. Greenblatt, E.C. Meng, and T.E. Ferrin. 2004. UCSF Chimera—a visualization system for exploratory research and analysis. *J. Comput. Chem.* 25:1605–1612. <https://doi.org/10.1002/jcc.20084>
- Pupo, A., D. Baez-Nieto, A. Martínez, R. Latorre, and C. González. 2014. Proton channel models filling the gap between experimental data and the structural rationale. *Channels (Austin)*. 8:180–192. <https://doi.org/10.4161/chan.28665>
- Qiu, F., A. Chamberlin, B.M. Watkins, A. Ionescu, M.E. Perez, R. Barro-Soria, C. González, S.Y. Noskov, and H.P. Larsson. 2016. Molecular mechanism of Zn<sup>2+</sup> inhibition of a voltage-gated proton channel. *Proc. Natl. Acad. Sci. USA*. 113:E5962–E5971. <https://doi.org/10.1073/pnas.1604082113>
- Ramsey, I.S., M.M. Moran, J.A. Chong, and D.E. Clapham. 2006. A voltage-gated proton-selective channel lacking the pore domain. *Nature*. 440: 1213–1216. <https://doi.org/10.1038/nature04700>
- Ramsey, I.S., Y. Mokrab, I. Carvacho, Z.A. Sands, M.S.P. Sansom, and D.E. Clapham. 2010. An aqueous H<sup>+</sup> permeation pathway in the voltage-gated proton channel Hv1. *Nat. Struct. Mol. Biol.* 17:869–875. <https://doi.org/10.1038/nsmb.1826>
- Randolph, A.L., Y. Mokrab, A.L. Bennett, M.S. Sansom, and I.S. Ramsey. 2016. Proton currents constrain structural models of voltage sensor activation. *eLife*. 5. e18017. <https://doi.org/10.7554/eLife.18017>
- Schrenzel, J., D.P. Lew, and K.H. Krause. 1996. Proton currents in human eosinophils. *Am. J. Physiol.* 271:C1861–C1871. <https://doi.org/10.1152/ajpcell.1996.271.6.C1861>
- Takeshita, K., S. Sakata, E. Yamashita, Y. Fujiwara, A. Kawanabe, T. Kurokawa, Y. Okochi, M. Matsuda, H. Narita, Y. Okamura, et al. 2014. X-ray crystal structure of voltage-gated proton channel. *Nat. Struct. Mol. Biol.* 21:352–357. <https://doi.org/10.1038/nsmb.2783>
- Thomas, R.C., and R.W. Meech. 1982. Hydrogen ion currents and intracellular pH in depolarized voltage-clamped snail neurones. *Nature*. 299: 826–828. <https://doi.org/10.1038/299826a0>
- Thomas, S., V.V. Cherny, D. Morgan, L.R. Artinian, V. Rehder, S.M.E. Smith, and T.E. DeCoursey. 2018. Exotic properties of a voltage-gated proton channel from the snail *Helisoma trivolvis*. *J. Gen. Physiol.* 150:835–850. <https://doi.org/10.1085/jgp.201711967>
- Tombola, F., M.H. Ulbrich, and E.Y. Isacoff. 2008. The voltage-gated proton channel Hv1 has two pores, each controlled by one voltage sensor. *Neuron*. 58:546–556. <https://doi.org/10.1016/j.neuron.2008.03.026>
- Tombola, F., M.H. Ulbrich, S.C. Kohout, and E.Y. Isacoff. 2010. The opening of the two pores of the Hv1 voltage-gated proton channel is tuned by cooperativity. *Nat. Struct. Mol. Biol.* 17:44–50. <https://doi.org/10.1038/nsmb.1738>
- van Keulen, S.C., E. Gianti, V. Carnevale, M.L. Klein, U. Rothlisberger, and L. Delemotte. 2017. Does proton conduction in the voltage-gated H<sup>+</sup> channel hHv1 involve Grotthuss-like hopping via acidic residues? *J. Phys. Chem. B*. 121:3340–3351. <https://doi.org/10.1021/acs.jpcc.6b08339>
- Webster, S.M., D. Del Camino, J.P. Dekker, and G. Yellen. 2004. Intracellular gate opening in Shaker K<sup>+</sup> channels defined by high-affinity metal bridges. *Nature*. 428:864–868. <https://doi.org/10.1038/nature02468>
- Wood, M.L., E.V. Schow, J.A. Freitas, S.H. White, F. Tombola, and D.J. Tobias. 2012. Water wires in atomistic models of the Hv1 proton channel. *Biochim. Biophys. Acta*. 1818:286–293. <https://doi.org/10.1016/j.bbame.2011.07.045>